OncoTargets and Therapy Dovepress

Open Access Full Text Article ORIGINAL RESEARCH

Utilizing Saliva Metabolomics for Diagnosing Gastric Cancer and Exploring the Changes in Saliva Metabolites After Surgery

Zhenhua Dong[1], Qirui Chen[2], Dingliang Zhao[3], Shaopeng Zhang[1], Kai Yu[4], Gaojun Wang[2], Daguang Wang[1]

[1]Department of Gastrointestinal Surgery, The First Hospital of Jilin University, Changchun, Jilin Province, 130000, People's Republic of China; [2]Undergraduate of Clinical Medicine, Jilin University, Changchun, Jilin, 130000, People's Republic of China; [3]Second Urology Department, The First Hospital of Jilin University, Changchun, Jilin Province, 130000, People's Republic of China; [4]Urology Department, The First Hospital of Jilin University, Changchun, Jilin Province, 130000, People's Republic of China

Correspondence: Daguang Wang, Department of Gastrointestinal Surgery, The First Hospital of Jilin University, Changchun, Jilin Province, 130000, People's Republic of China, Tel/Fax +86 18743066256, Email dgwang@jlu.edu.cn

Purpose: Gastric cancer (GC) is a disease with high prevalence and mortality, but we lack convenient and accurate methods to screen for this disease. Thus, we aimed to search for some salivary biomarkers and explore changes in metabolites in patients' saliva after radical gastrectomy.

Patients and Methods: A total of 152 subjects were divided into three groups (healthy group, GC group, and one-week post-operative group). After simple processing, saliva samples were analyzed by liquid chromatography–mass spectrometry. First, we used total ion chromatography and principal component analysis to determine the metabolite profiles. Next, *t*-test, partial least squares discriminant analysis, support vector machine, and receiver operating characteristics curve analysis were performed to identify biomarkers. Then, Fisher discriminant analysis and hierarchical clustering analysis were performed to determine the discriminating ability of biomarkers. Finally, we established a generalized linear model to predict GC based on biomarkers, and used bootstrapping for internal validation.

Results: Between the healthy and GC groups, we identified four biomarkers: lactic acid, kynurenic acid, 3-hydroxystachydrine, and S-(1,2,2-trichlorovinyl)-L-cysteine. We used stepwise regression to select five metabolites and develop a model with areas under the curve equal to 0.973 in the training dataset and 0.924 in the validation dataset. Between the GC and one-week postoperative groups, we found two differential metabolites: 19-hydroxyprostaglandin E_2 and DG (14:0/0:0/18:2n6).

Conclusion: Differential metabolites were observed among the three groups. GC could be initially diagnosed on the basis of detection of these biomarkers. Moreover, changes in salivary metabolites in postoperative patients could provide important insights for basic studies.

Keywords: liquid chromatography–mass spectrometry, saliva, gastric cancer, postoperative patients, clinical prediction model

Introduction

There are 990,000 people diagnosed with gastric cancer (GC) and 738,000 deaths every year. GC is the fourth most common cancer and the second most frequent reason for death related to cancer.[1] The reason for this is partly because it lacks specific symptoms and is always at a late stage when diagnosed. In Japan, since 1960, there has been mass screening for GC using photofluorography, and the 5-year survival rate in screening-detected cases has increased by 15–30% compared with symptom-diagnosed cases,[2] which shows that early diagnosis of GC is essential. Currently, gastroscopy and tissue biopsy are the gold standards for GC diagnosis, but these tests are expensive and can have a negative effect on patients' mood.[3] Computed tomography (CT) is a common imaging examination, but it is insensitive to early GC and may cause radical damage. Lastly, serum tumor markers possess low specificity for GC. Therefore, safe, accurate, cheap, non-invasive, and repeatable methods for identifying GC are paramount.

Received: 26 July 2024
Accepted: 3 October 2024
Published: 6 November 2024

People usually produce 0.5–1.5 L saliva per day, which is composed of 99% water, less than 1% protein, and low-molecular-weight substances.[4] Saliva plays an important role in maintaining oral health. Cancer-derived exosomes containing rich genetic information about the cancer can reach the salivary glands through the blood circulation, thus reflecting the close relationship between cancer and saliva.[5] Salivaomics has identified many biomarkers for several diseases, such as oral cancer, pancreatic cancer,[6] breast cancer, and periodontal disease.[7] Some researchers have found that the physical components of saliva are close to those of serum.[8] Compared with serum, saliva is easier to obtain repeatedly. Thus, we conducted the present experiments using salivary samples.

Following genomics, transcriptomics, and proteomics, metabolomics has huge potential to discover complex pathogenesis by focusing on low-molecular-weight compounds.[9] Liquid chromatography–mass spectrometry (LC-MS) is one of the main methods used for metabolomic measurement, and possesses strengths of high sensitivity, specificity, and resolution. In this study, we utilize LC-MS to seek biomarkers for GC, identify differential metabolites between GC and one-week postoperative patients, and explore whether there is a change in metabolites among different T stages, with the final goal of improving patients' prognoses.

Materials and Methods

Patients

This study was approved by the Ethics Committee of The First Hospital of Jilin University and all patients provided signed informed consent forms. All study procedures satisfied ethical rules. All saliva samples were collected from patients with pathologically supported GC who underwent treatment at the Department of Gastrointestinal Surgery, The First Hospital of Jilin University (China), in June 2024. This study consisted of 152 samples divided into three groups, comprising the healthy group (47), GC group (51), and one-week postoperative group (54). The inclusion criteria for the healthy group were: people with normal results on routine blood and urine examinations, liver and renal function, electrocardiogram, and CT. The exclusion criteria for the healthy group, GC group, and one-week postoperative group were as follows: (1) people with congenital disease; (2) people with metabolic diseases (eg, diabetes or obesity); (3) women who were pregnant or breastfeeding; (4) people with alcoholism or drug abuse, including steroid hormones or analgesics; (5) people with inflammation (eg respiratory or urinary system); (6) people who encountered a large stress response during one month; (7) people with any blood or oral diseases; and (8) people whose gastroscope results showed common gastric diseases (eg atrophic gastritis or gastric ulcer). Inclusion criteria for the GC group were: (1) postoperative pathological results of gastric adenocarcinoma; (2) no history of tumor, radiotherapy, or chemotherapy; (3) good bone marrow, liver, and renal function; and (4) absence of evident acute inflammation and oral diseases. The inclusion criteria for the one-week postoperative group are the same as those for the GC group as well as up to one week after radical gastrectomy.

To avoid the influence of other confounding factors, we collected the same patients' saliva before and after surgery, which means that patients overlapped between the GC group and one-week postoperative group. Because the patients had gone without water before surgery and owing to our lack of experience in the early stages of the study, the volume of saliva collected from three GC patients was too small to perform further analyses and we abandoned these three samples (B1, B2, B5). However, saliva samples collected from these three patients after surgery were still included in our study (C1, C2, C5), which is why the GC group has 51 and the one-week postoperative group has 54 samples.

Sample Collection and Processing

All saliva samples are collected from subjects who had abstained from smoking, drinking, eating, toothbrushing, or using drugs, between 7 and 8 am. After the participants had gargled with distilled water three times, we waited 10 min and then collected saliva using collectors (Salivette, Germany). We transported the samples at −20°C within 1 h, centrifuged them at 4000 rpm for 2 min at 4°C, and extracted the upper fluid into 2 mL Eppendorf tubes, which were stored in a refrigerator at −80°C for subsequent analysis.

After samples had been thawed at 4°C, we drew 20 μL saliva from each sample into a 5 mL Eppendorf tube, for use as a quality control (QC). The procedure for the QC was the same as for the other samples. First, we drew 100 μL saliva

from each tube into a 96-well plate, and mixed it with 300 μL methanol. Second, the 96-well plate was vortexed for 6 min and left to stand at 4°C for 10 min, to allow the proteins to precipitate fully. Third, we blew the 96-well plate with nitrogen until all fluid had evaporated. Fourth, 100 μL methanol:water (1:1, v/v) was injected into the 96-well plate and we transferred the sample into a 2 mL Eppendorf tube for further centrifugation (15,000 rpm, 4°C, 10 min). Fifth, 75 μL supernatant fluid was drawn from each tube for LC-MS.

Liquid Chromatography

The Exion UHPLC system (Shimadzu, Japan) was used for LC-MS. Samples were mixed by a Vortex 3 (IKA, Germany) and centrifuged at 4°C by the H165R centrifuge (Xiangyi Centrifuge Instrument Co., China). Solvents included acetonitrile (HPLC grade, Sigma-Aldrich, USA), formic acid (HPLC grade, Sigma-Aldrich, USA), methanol (HPLC grade, Merck, Germany), and deionized water (Watson, China). We utilized APCI positive and negative calibration solution (AB Sciex) to perform ion calibration. The column temperature was set to 35°C (Acquity UPLC HSS T3, 2.1×100 mm, 1.8 μm, Waters, USA). The mobile phase was composed of the A phase (0.1% formic acid and water) and B phase (acetonitrile). Before analysis, the initial mobile phase was balanced for 5 min to make the system more stable. Then, 10 QCs were analyzed initially for the same purpose. We set the flow rate to 0.3 mL/min and the sample volume to 0.5 μL. The gradient times were as follows: 0.3 and 1 min (A phase 99% + B phase 1%); 8 and 9.5 min (A phase 1% + B phase 99%); 9.6 and 13 min (A phase 99% + B phase 1%).

Mass Spectrometry

We utilized a Triple TOF 5600TM system (AB Sciex) with an electrospray ionization source for MS. The first-level MS parameters included: in the positive model, the ion spray voltage (V) was set to 5500, temperature (°C) to 550, gas 1 (psi) to 55, gas 2 (psi) to 55, curtain gas (psi) to 30, declustering potential (DP) to 100, and collision energy (CE) to 10; while in the negative model, the ion spray voltage (V) was changed to −4500, DP to −100, and CE to −10, and the remaining parameters were the same. The second-level mass spectrometry parameters included: in the positive model, the ion spray voltage (V) was set to 5500, temperature (°C) to 550, gas 1 (psi) and gas 2 (psi) to 55, curtain gas (psi) to 30, DP to 100, CE to 35, collision energy spread (CES) to 15, ion release delay (IRD) to 67, and ion release width (IRW) to 25; while in the negative model, the ion spray voltage (V) was changed to −4500, DP to −100, and CE to −35, and the remaining parameters were the same. The TOF-MS-IDA model was used to collect data. The scan range of MS varied from 50 to 1500 Da.

Statistical Analysis

First, raw data were converted to wiff file format using Analyst TF 1.7.1, and total ion chromatography (TIC) graphs were drawn using PeakView 2.2. With the help of Dalian ChemDataSolution Information Technology Co. (China), data were further transformed into Excel form. After standardization, normalization, noise filtering, and peak alignment, we performed *t*-tests and partial least squares discriminant analysis (PLS-DA) using MetaboAnalyst 6.0. Metabolites with false discovery rate <0.05 and variable important in projection (VIP) values >1.2 were selected. Next, we utilized R studio to run the support vector machine (SVM) and chose metabolites with 100% weight for sample classification.

If there was no severe collinearity (variance inflation factor [VIF] <10) among metabolites, we performed Fisher discriminant analysis to calculate sensitivity and specificity using SPSS. Based on the mass-to-charge ratio, we searched the Human Metabolome Database (HMDB) for specific metabolite information. Hierarchical clustering analysis (HCA) was used to test the discriminant ability of many metabolites, and receiver operating characteristics (ROC) curve analysis to test the discriminant ability of a single metabolite. Lastly, trends in the change of metabolites within two groups are shown as scatterplots.

Between the healthy and GC groups, stepwise regression was utilized to filter the metabolites until the smallest Akaike information criterion (AIC) was achieved. Based on the selected metabolites, we established a generalized linear model (GLM) to predict GC. Owing to the limited sample size, bootstrapping was applied for the internal validation. The AIC, area under the curve (AUC), and calibration curve were used to evaluate model performance. If the Hosmer and Lemeshow goodness of fit (GOF) test $P<0.05$, a statistical difference between the actual and predicted values was noted.

Packages including "peatmap", "ggplot2", "e1071", "glmnet", "gtsummary", and "ResourceSelection" in R 4.3.1, SPSS 27.0, and MetaboAnalyst 6.0 are used in this study.

Results

Healthy Group and GC Group

TIC shows differences in peak intensity at the same retention time in positive and negative models, which indicate that there are differential metabolites between the healthy and GC groups (Figure 1a–d). In principal component analysis (PCA), each plot represents a sample and these plots can be roughly divided into two parts (Figure 2a and b). The plots within a group are close and those among groups are distant, which suggests that differences in metabolites within a group are small and those between groups are large. The QCs gathered well. Therefore, all study data are reliable.

After the *t*-test ($P<0.05$), 1119 metabolites (positive model) and 526 metabolites (negative model) were selected, as shown in Figure 2c and d, respectively (Table S1). In volcano plots, the brighter the color, the smaller the *P* value, and gray plots do not show statistical differences between groups. We performed PLS-DA for further filtering and obtained 31 metabolites with VIP >1.2 (Figure 3a) (Table S2). Based on these 31 metabolites, the PLS-DA plot is protracted and shows that two groups can be clearly separated (Figure 3b). After SVM, we obtained eight metabolites with weights approaching 100%. According to their mass-to-charge ratio, we determined the chemical names and structures in HMDB, as lactic acid, S-(1,2,2-trichlorovinyl)-L-cysteine, 3-hydroxystachydrine, kynurenic acid, calcium, L-glyceric acid, PE (20:2(11Z,14Z)/P-18:1(9Z)), and adenosyl cobinamide (Table 1).

The VIF <10 of eight metabolites shows that the collinearity is small (Table S3). From the Fisher analysis, the true positive is 44, false negative is 7, true negative is 40, and false positive is 7, so the sensitivity is 86.3% and specificity is 85.1%. Next, we conducted HCA and plotted a heatmap based on the eight metabolites, in which the color intensity represents the content of metabolites in samples and the dendritic structure above the picture suggests the similarity of samples. Overall, these samples could be regrouped correctly in the heatmap (Figure 3c). Finally, we chose four metabolites as possible biomarkers through ROC curve analysis, comprising AUC >0.8 (lactic acid, 3-hydroxystachydrine) and AUC <0.2 (kynurenic acid, S-(1,2,2-trichlorovinyl)-L-cysteine)) (Figure S1) (Table 2). Compared with the

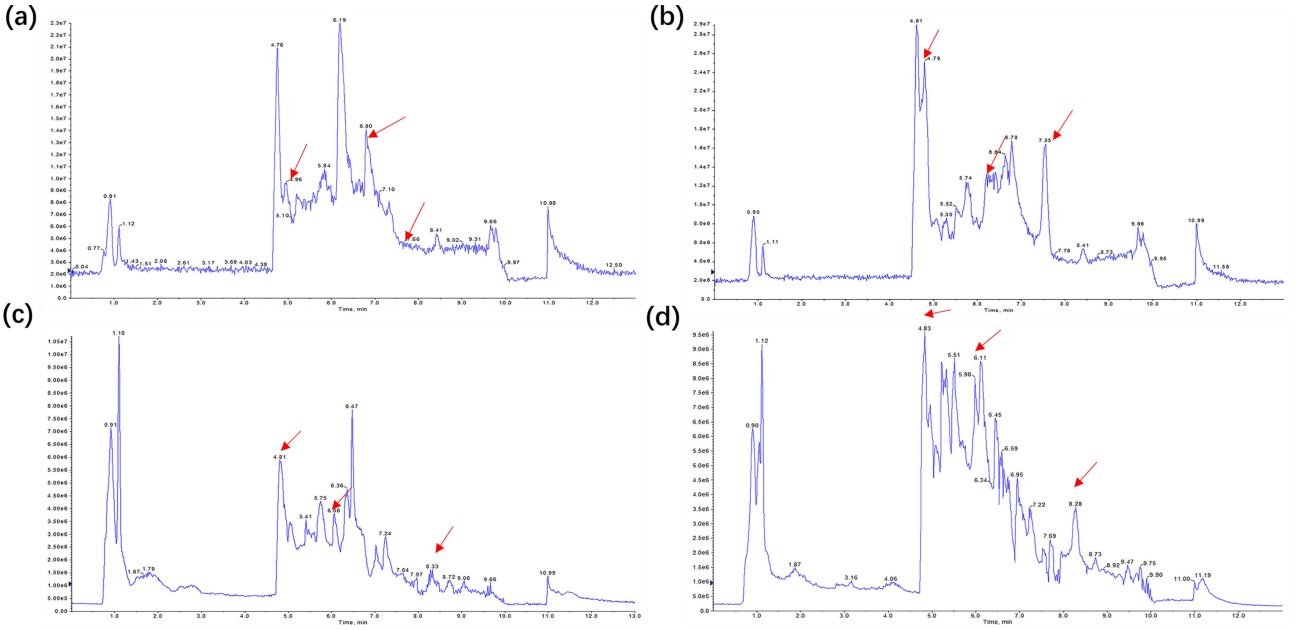

Figure 1 TIC chromatograms of metabolites of samples from the healthy group and GC group. (**a**) TIC profiles of healthy group in the positive ion mode; (**b**) TIC profiles of GC group in the positive ion mode; (**c**) TIC profiles of healthy group in the negative ion mode; (**d**) TIC profiles of GC group in the negative ion mode. Red arrows indicate metabolites subsequently identified as having different abundances in the two groups. The vertical coordinate is the time; the horizontal coordinate is the intensity of metabolite.

Abbreviations: TIC, total ion chromatography; GC, gastric cancer.

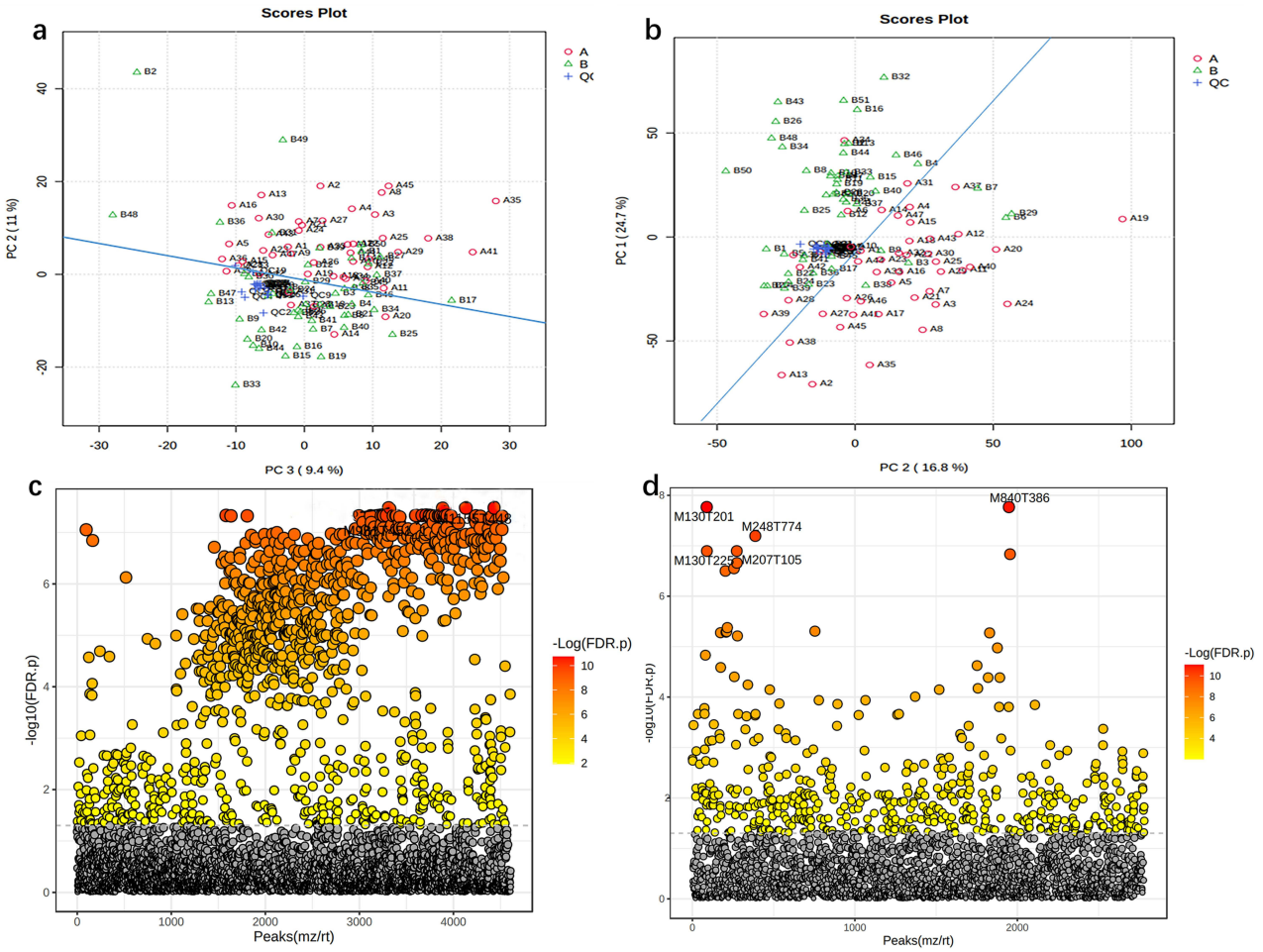

Figure 2 *t*-Test and principal component analysis of samples from the healthy group and GC group. (**a**) Principal component analysis in the positive ion mode; (**b**) principal component analysis in the negative ion mode; each dot represents a single sample; (**c**) *t*-test in the positive ion mode; (**d**) *t*-test in the negative ion mode. The vertical coordinate is the *P* value, the horizontal coordinate is the level of each metabolite, and orange represents the significant metabolites, with $P<0.05$.
Abbreviations: GC, gastric cancer; A, healthy group; B, GC group; QC, quality control group.

healthy group, the density of lactic acid and 3-hydroxystachydrine increased, while kynurenic acid and S-(1,2,2-trichlorovinyl)-L-cysteine decreased in the GC group (Figure 4a–d).

Five of the eight metabolites were selected by stepwise regression to fit the model with an AIC of 52.712 and an AUC of 0.973 (Figure 5a). Lactic acid, 3-hydroxystachydrine, and PE (20:2(11Z,14Z)/P-18:1(9Z)) were positively associated with GC. For every increase of 1000 units of lactic acid and PE(20:2(11Z,14Z)/P-18:1(9Z)), the risk of GC increased by 1.47% (95% confidence interval [CI], 0.45–3.33), 1.02% (95% Cl, 0.06–2.24%), and 3.49% (95% Cl, 0.95–7.26%), respectively. S-(1,2,2-Trichlorovinyl)-L-cysteine and kynurenic acid were negatively associated with GC. For every increase of 1000 units of S-(1,2,2-trichlorovinyl)-L-cysteine and kynurenic acid, the risk of GC decreased by 0.83% (95% Cl, 0.23–1.65%) and 0.54% (95% Cl, 0.09–1.14%), respectively (Table 3). The calibration curve shows that the difference between the actual value (dotted line) and the ideal value (solid line) is small, and the GOF test ($P=0.63$, >0.05) supports this conclusion (Figure 5b). In decision curve analysis, we observe that the net benefit of our model is always higher than none or all lines' net benefit within the threshold probability between 0 and 1, which suggests that our model has potential value for practical use (Figure 5c). We performed 100 times bootstrapping to validate this model, and the average AUC=0.924, which shows that our model possesses excellent performance (Figure 5d).

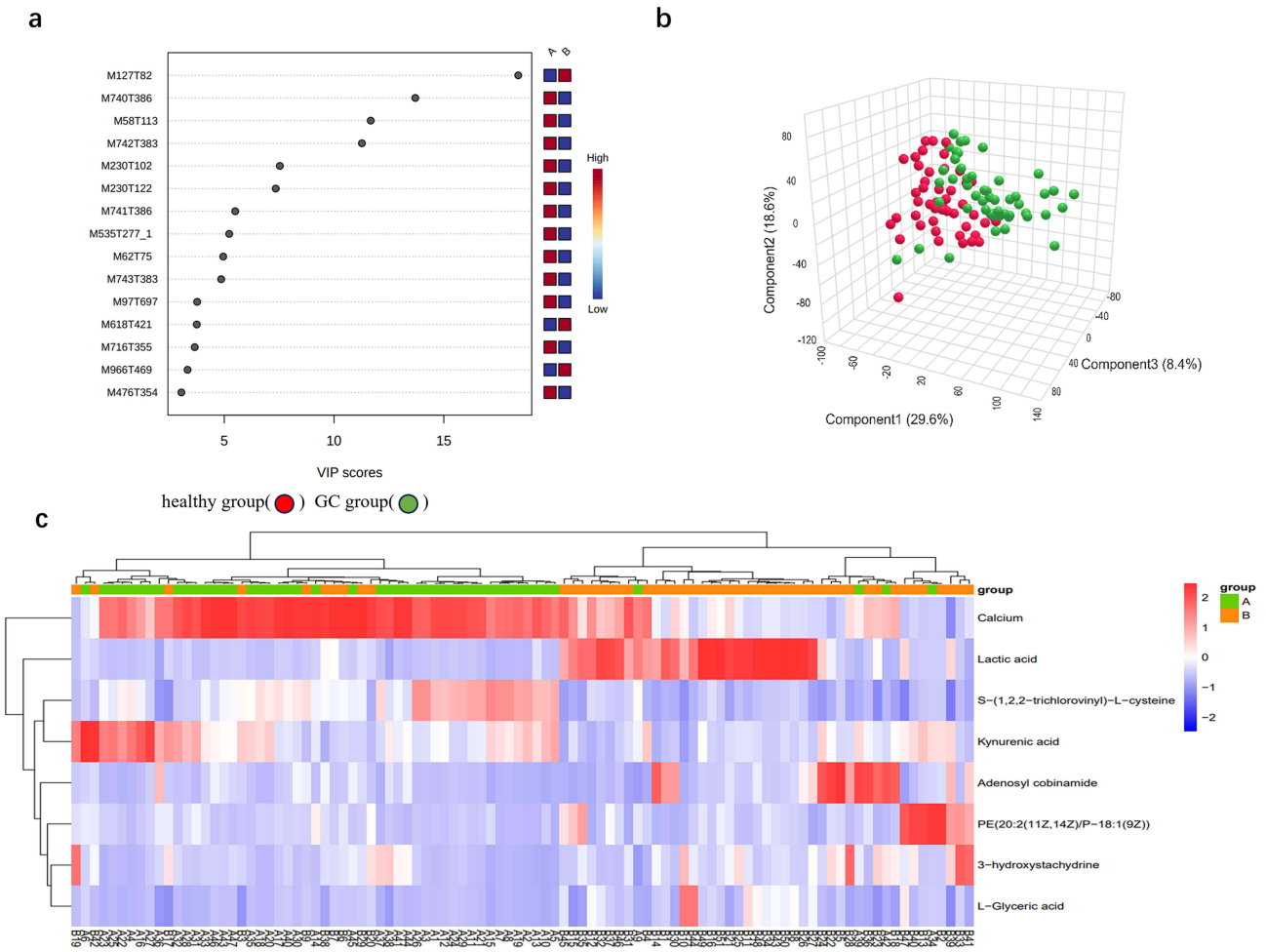

Figure 3 VIP score plot, PLS-DA plot, and clustering analysis of samples from the healthy group and GC group in positive and negative models. (**a**) VIP score plot for the selected differential metabolites with VIP >1.2; (**b**) PLS-DA plot; (**c**) hierarchical clustering analysis of the eight differential metabolites. The color scale represents the relative abundance of metabolites, with red indicating higher abundance, white indicating zero abundance, and blue indicating lower abundance. The right side of the figure shows the peak name of each metabolite, while the dendrogram on the left and top represents the clustering results of the differential metabolites. The sample numbers are shown at the bottom of the figure.

Abbreviations: VIP, variable importance in projection; PLS-DA, partial least squares discriminant analysis; GC, gastric cancer; A, healthy group; B, GC group.

GC and One-Week Postoperative Group

TIC indicates that there are differential metabolites between the GC and one-week postoperative groups (Figure 6a–d). Based on PCA2 (16.5%) and PCA3 (8.4%) in the positive model, and PCA1 (20.7%) and PCA2 (16.6%) in the negative model, these plots

Table 1 Metabolites Identified that Differentiate Between Healthy Group and GC Group

Ionization	Peak Name	Mass-to-Charge Ratio	Chemical Formula	Metabolite
ESI−	M127T82	126.9046	$C_3H_6O_3$	Lactic acid
ESI−	M230T102	229.8616	$C_5H_6Cl_3NO_2S$	S-(1,2,2-Trichlorovinyl)-L-cysteine
ESI−	M180T246	180.0673	$C_7H_{13}NO_3$	3-Hydroxystachydrine
ESI−	M62T75	61.9882	$C_{10}H_7NO_3$	Kynurenic acid
ESI−	M58T113	57.9757	Ca	Calcium
ESI−	M127T62	126.905	$C_3H_6O_4$	L-Glyceric acid
ESI+	M761T590	760.58	$C_{43}H_{80}NO_8P$	PE(20:2(11Z,14Z)/P-18:1(9Z))
ESI−	M618T421	617.7198	$C_{58}H_{85}CoN_{16}O_{14}P$-2	Adenosyl cobinamide

Abbreviation: GC, gastric cancer.

Table 2 AUC of Differential Metabolites Between Healthy Group and GC Group.

Metabolites	AUC	SE	95% Confidence Intervals	
			Lower	Upper
Lactic acid	0.845	0.044	0.759	0.932
Adenosyl cobinamide	0.739	0.050	0.641	0.837
L-Glyceric acid	0.785	0.046	0.694	0.875
Calcium	0.211	0.047	0.118	0.304
Kynurenic acid	0.187	0.043	0.102	0.272
PE(20:2(11Z,14Z)/P-18:1(9Z))	0.713	0.051	0.612	0.813
3-hydroxystachydrine	0.819	0.044	0.732	0.905
S-(1,2,2-trichlorovinyl)-L-cysteine	0.165	0.041	0.085	0.245

Abbreviation: GC, gastric cancer; AUC, area under the curve.

could be separated into two groups (Figure 7a and b). The QCs assemble well, which suggests that the LC-MS system is stable. After the *t*-test ($P<0.05$), 2722 metabolites (positive model) and 988 metabolites (negative model) were selected, as shown in Figure 7c and d, respectively (Table S4). In PLS-DA, we obtained 74 metabolites with VIP >1.2 (Figure 8a) (Table S5). We drew a PLS-DA plot based on 74 metabolites, which demonstrates that two groups can be divided roughly (Figure 8b). After SVM, we obtained six metabolites with a weight approaching 100%. According to the mass-to-charge ratio, we determined the chemical names and structures in HMDB, as ganglioside GD2 (d18:1/16:0), DG(14:0/0:0/18:2n6), 19-hydroxyprostaglandin E_2, delta-N-methylarginine, cis-inositol, and LysoPI(18:1(9Z)/0:0) (Table 4).

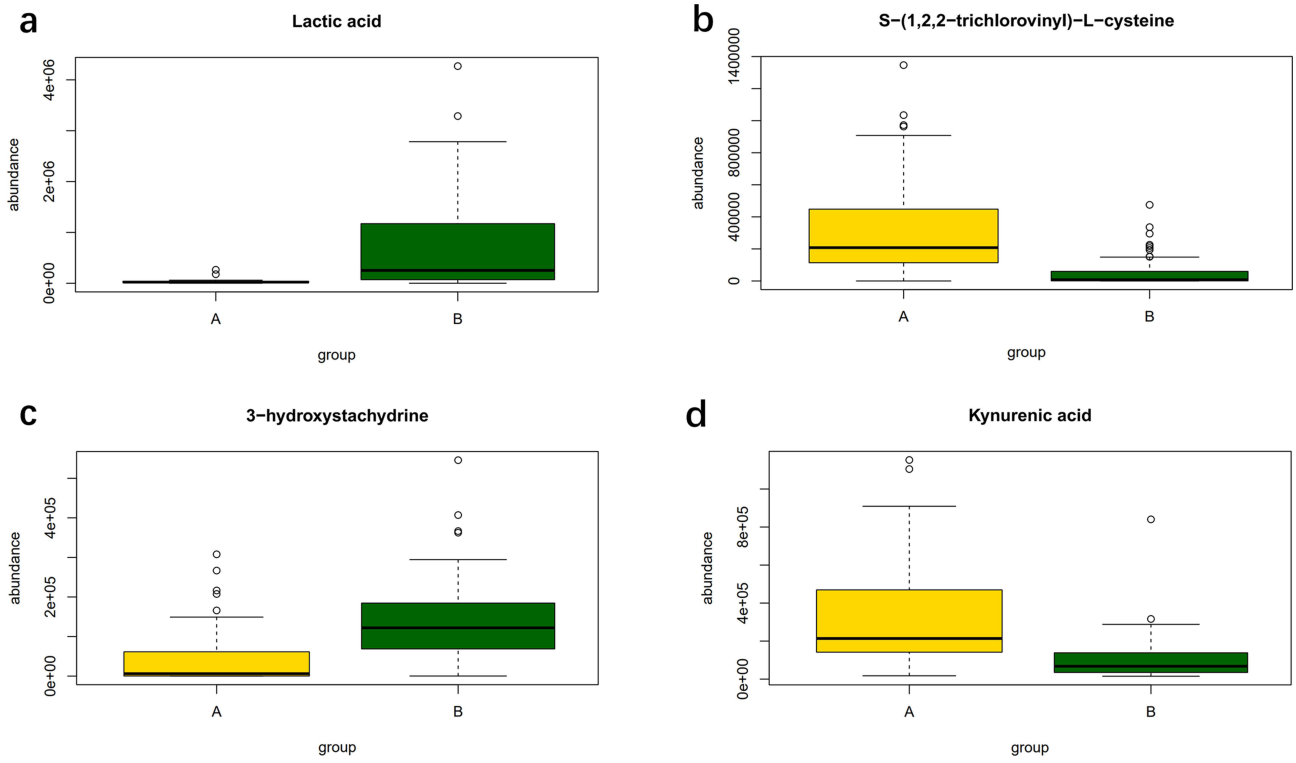

Figure 4 Mean plots of four differential metabolites between the healthy group and GC group. (**a**) Lactic acid; (**b**) S-(1,2,2-trichlorovinyl)-L-cysteine; (**c**) 3-hydroxystachydrine; (**d**) kynurenic acid.
Abbreviations: GC, gastric cancer; A, healthy group; B, GC group.

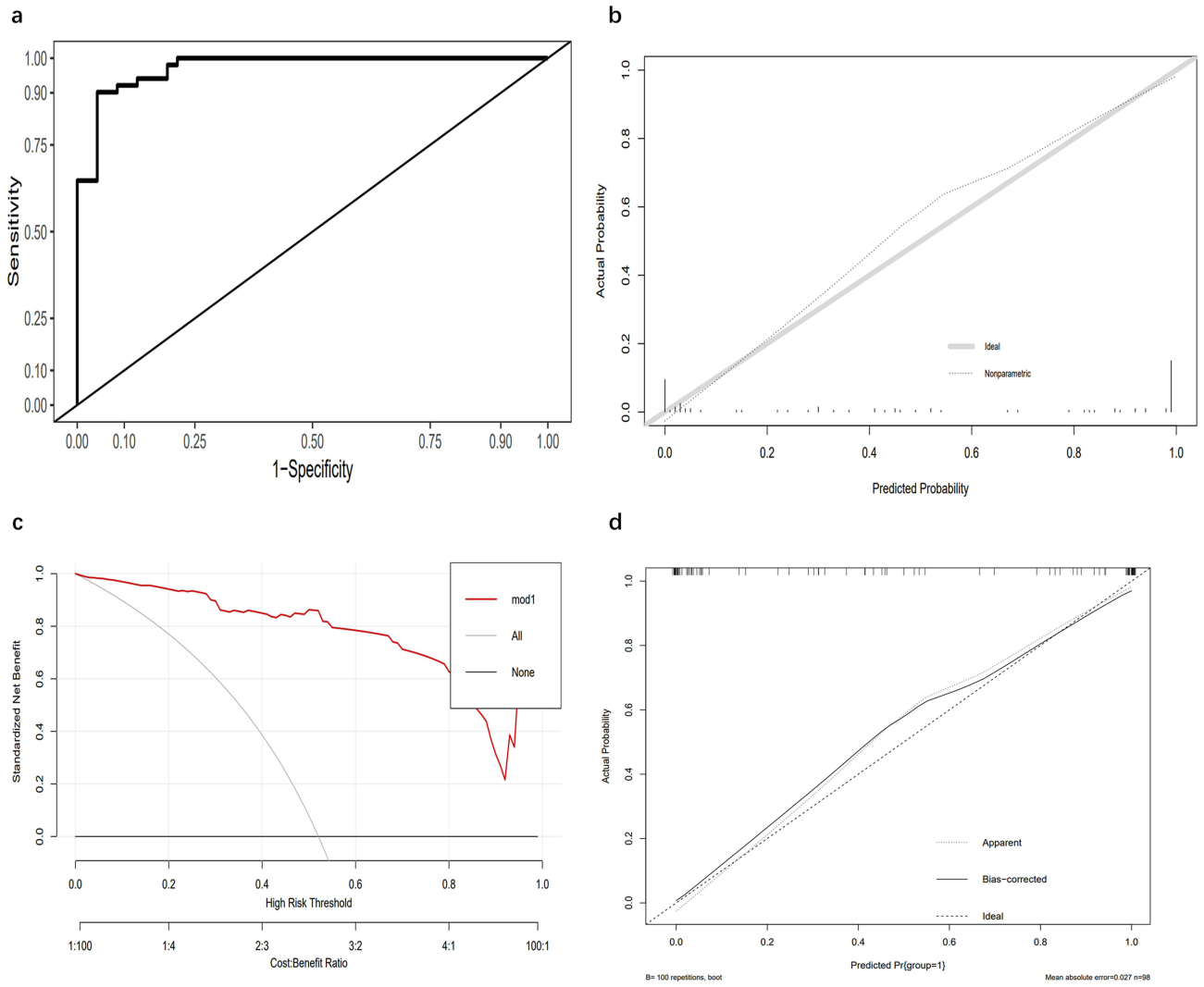

Figure 5 ROC curve, calibration curve, decision curve analysis, and bootstrap curve of the prediction model. (**a**) ROC curve with AUC=0.973; (**b**) calibration curve, with solid line representing ideal value and dotted line representing actual value; (**c**) decision curve analysis; (**d**) 100 times bootstrap curve with AUC=0.924.
Abbreviations: ROC, receiver operating characteristics; AUC, area under the curve.

The VIF <10 of six metabolites shows that the collinearity is acceptable (Table S6). In the Fisher analysis, the true positive is 46, false negative is 5, true negative is 47, and false positive is 7, so the sensitivity is 87% and specificity is 90.2%. In the heatmap (Figure 8c), GC and almost half of the one-week postoperative patients form a cluster, and then

Table 3 Variants Information in the Prediction Model

Metabolites	Beta	Z Value	OR	OR (95% CI)	P Value
Intercept	−2.3176	−2.045	0.0985	(0.0079, 0.7540)	0.0409
Lactic acid	0.0145	2.11	1.0147	(1.0045, 1.0333)	0.0348
S-(1,2,2-Trichlorovinyl)-L-cysteine	−0.0082	−2.326	0.9917	(0.9835, 0.9977)	0.02
3-Hydroxystachydrine	0.0101	1.896	1.0102	(1.0006, 1.0224)	0.0579
Kynurenic acid	−0.0053	−2.048	0.9946	(0.9886, 0.9991)	0.0406
PE(20:2(11Z,14Z)/P-18:1(9Z))	0.0344	2.266	1.0349	(1.0095, 1.0726)	0.0235

Abbreviations: OR, odds ratio; CI, confidence interval.

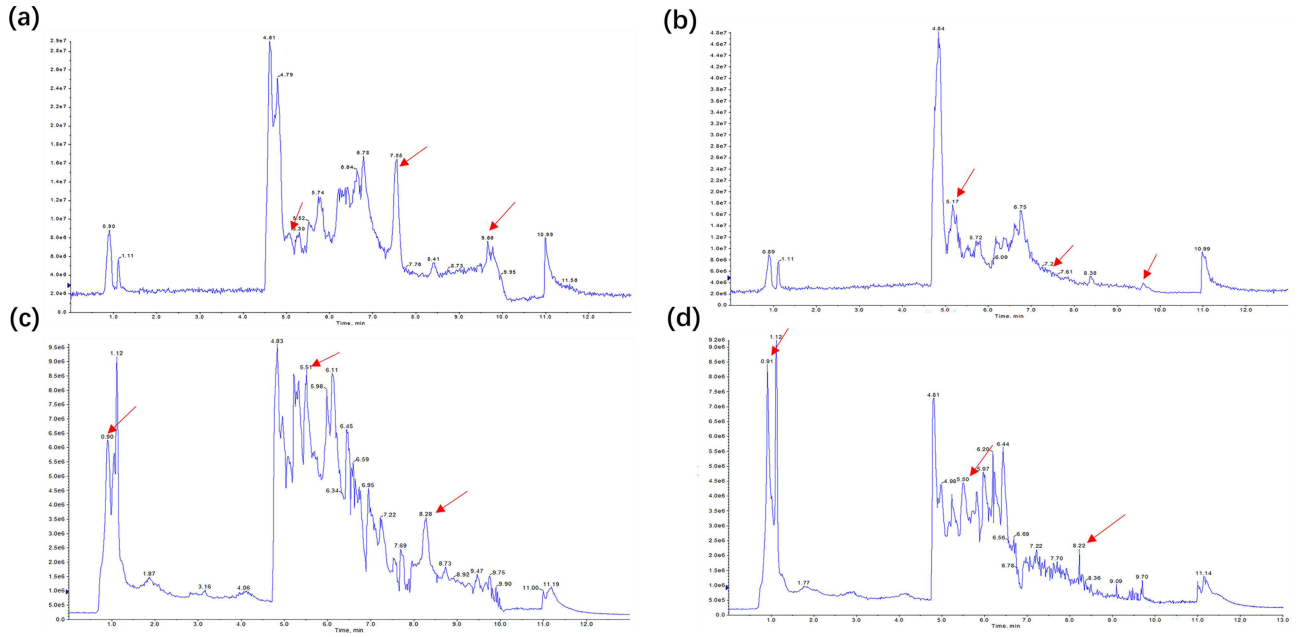

Figure 6 TIC chromatograms of metabolites of samples from the GC group and one-week postoperative group. (**a**) TIC profiles of GC group in the positive ion mode; (**b**) TIC profiles of TIC profiles of one-week postoperative group in the positive ion mode; (**c**) TIC profiles of GC group in the negative ion mode; (**d**) TIC profiles of one-week postoperative group in the negative ion mode. Red arrows indicate metabolites subsequently identified as having different abundances in the two groups.
Abbreviations: TIC, total ion chromatography; GC, gastric cancer.

they become a large cluster with the rest of the one-week postoperative patients. Although patients cannot be separated into two groups directly, we still believe that these six metabolites have discriminant ability, to some extent. Finally, we chose two metabolites through ROC curve analysis, comprising AUC=0.9 (19-hydroxyprostaglandin E_2) and AUC=0.1 (DG(14:0/0:0/18:2n6)) (Figure 9a) (Table 5). Compared with GC, the density of DG(14:0/0:0/18:2n6) increased, while 19-hydroxyprostaglandin E_2 decreased in the one-week postoperative group (Figure 9b and c).

Regrouping GC According to Different T and N Stages

After inspecting the postoperative pathology of each patient, we found T1 (12), T2 (8), T3 (16), and T4 (15). Next, the GC group was further divided into four groups. In PCA, these four groups could not be separated (Figure 10a and b). We performed analysis of variance in MetaboAnalyst 6.0, but the results showed that there are no differential metabolites among the four groups (Figure 10c and d). Based on the postoperative pathology of the patients, we identified N0 (19), N1 (9), N2 (16), N3a (7), and N3b (10). Then, we separated GC patients into five groups. In PCA, these five groups also could not be separated clearly (Figure 11a and b). We performed analysis of variance, but the results show that there are no differential metabolites among the five groups (Figure 11c and d).

Therefore, we discovered that the salivary metabolites of patients at different tumor T and N stages may be similar. However, more studies are needed to validate this conclusion because of the limited sample size in this work.

Discussion

In this study, we utilized LC-MS metabolomics to analyze salivary samples, and found four metabolites that could be used as possible tumor biomarkers for GC and two differential metabolites between GC and one-week postoperative groups. Based on five metabolites, we have developed a GLM with good performance to predict GC. However, we hold that salivary metabolites cannot convey information about GC T stages.

We will discuss the association between seven metabolites and GC. First, lactic acid is an organic acid, which plays a role in several biochemical processes. For maintaining the rapid growth of GC cells, providing raw materials for cell division and balancing redox homeostasis in GC cells, metabolic reprogramming occurs in GC and glycolysis becomes a main pathway to produce energy.[10] Glycolysis can create an enormous amount of lactic acid, which activates mesenchymal stem cells (MSCs)

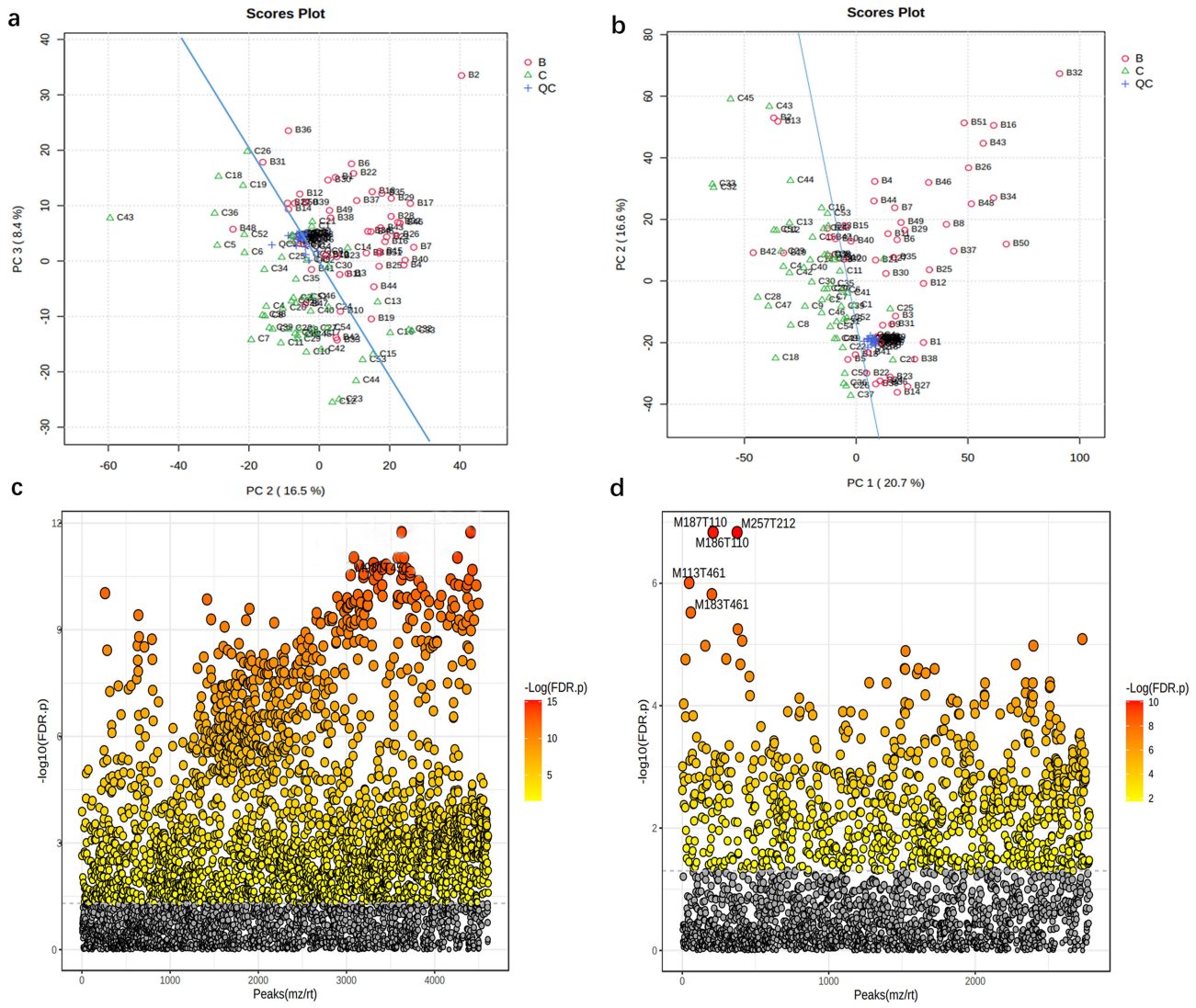

Figure 7 *t*-Test and principal component analysis of samples from the GC group and one-week postoperative group. (**a**) Principal component analysis in the positive ion mode; (**b**) principal component analysis in the negative ion mode; each dot represents a single sample; (**c**) *t*-test in the positive ion mode; (**d**) *t*-test in the negative ion mode. **Abbreviations**: GC, gastric cancer; B, GC group. C, one-week postoperative group; QC, quality control group.

constituting GC stroma through monocarboxylate transporter-1/transforming growth factor-beta-1 signaling.[11] MCSs can increase the expression of programmed death ligand-1 to prompt the migration of GC,[12] which may explain why the content of lactic acid in GC cells increases. Second, S-(1,2,2-trichlorovinyl)-L-cysteine belongs to the class of organic compounds known as cysteine and derivatives. A prospective study recruiting more than 1000 people found that the cysteine content in serum is negatively associated with the risk of gastric cardia adenocarcinomas, because cysteine regulates many immune pathways and possesses antioxidant functions.[13] Previous animal research found that cysteine can inhibit human SJ-89 cells (GC) by decreasing DNA synthesis and increasing cell apoptosis,[14] which may support the finding that the content of S-(1,2,2-trichlorovinyl)-L-cysteine is decreased in GC. Third, 3-hydroxystachydrine belongs to the class of organic compounds known as proline and derivatives. In 2024, Liu et al used an enantiomer-specific colorimetric tandem to measure proline in saliva, and their results indicated that the level of proline in GC is significantly higher than in healthy saliva, which validates our conclusion.[15] Proline metabolism is essential for GC cell proliferation, survival, and metastasis because it can produce enough protein, providing material of rapid cell growth,[16] decrease the generation of ROS to increase the GC cell survival rate, and change the expression of relevant genes to prompt cancer cell invasion into other tissues,[17] which may explain why 3-hydroxystachydrine increases in GC. Fourth, kynurenic acid has anti-tumor functions because it can inhibit GC

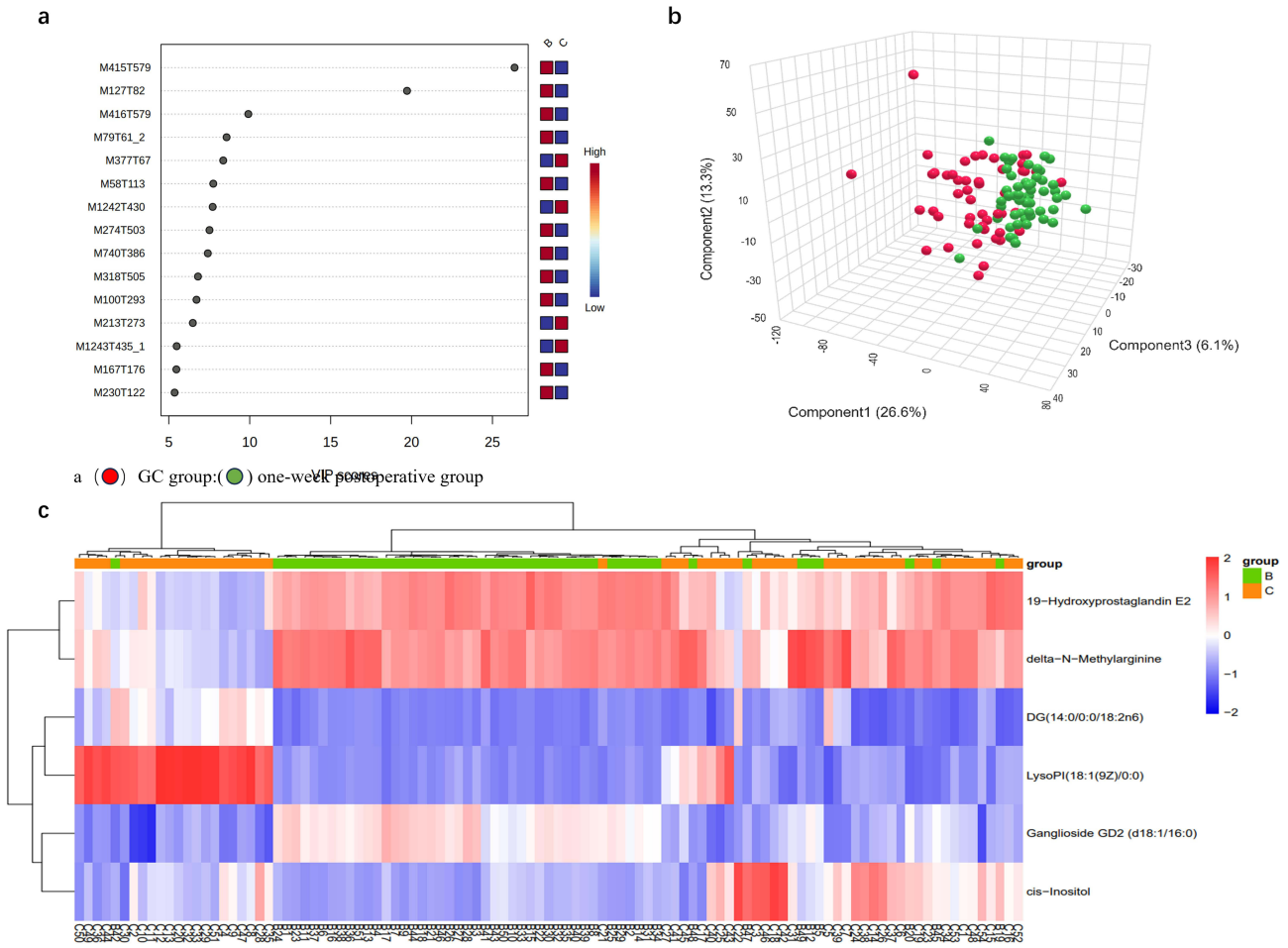

Figure 8 VIP score plot, PLS-DA plot, and clustering analysis of samples from the GC group and one-week postoperative group in positive and negative models. (**a**) VIP score plot for the selected differential metabolites with VIP >1.2; (**b**) PLS-DA plot; (**c**) hierarchical clustering analysis of the six differential metabolites.
Abbreviations: VIP, variable importance in projection; PLS-DA, partial least squares discriminant analysis; GC, gastric cancer; B, GC group; C, one-week postoperative group.

growth via the PI3K/AKT and MAPK pathways[18] and induce AGS (GC cell) apoptosis,[19] which explains why the kynurenic acid level decreases in GC. Based on LC-MS, Choi et al utilized tryptophan and its seven metabolites, including kynurenic acid, in GC serum to establish a prediction model, which indicates that kynurenic acid is a potential biomarker for GC.[20] Fifth, PE(20:2(11Z,14Z)/P-18:1(9Z)) is a phosphatidylethanolamine. Based on serum metabolomics, previous research found that

Table 4 Metabolites Identified that Differentiate Between GC Group and One-Week Postoperative Group

Ionization	Peak Name	Mass-to-Charge Ratio	Chemical Formula	Metabolite
ESI+	M846T579	846.4416	$C_{76}H_{134}N_4O_{34}$	Ganglioside GD2 (d18:1/16:0)
ESI−	M1202T372	1202.0482	$C_{36}H_{66}O_5$	DG(14:0/0:0/18:2n6)
ESI+	M432T579	432.2371	$C_{20}H_{32}O_6$	19-Hydroxyprostaglandin E_2
ESI+	M415T565	415.2106	$C_7H_{16}N_4O_2$	Delta-N-Methylarginine
ESI−	M89T112	89.0244	$C_6H_{12}O_6$	cis-Inositol
ESI−	M1242T436	1241.5299	$C_{27}H_{51}O_{12}P$	LysoPI(18:1(9Z)/0:0)

Abbreviation: GC, gastric cancer.

https://doi.org/10.2147/OTT.S482767 DovePress

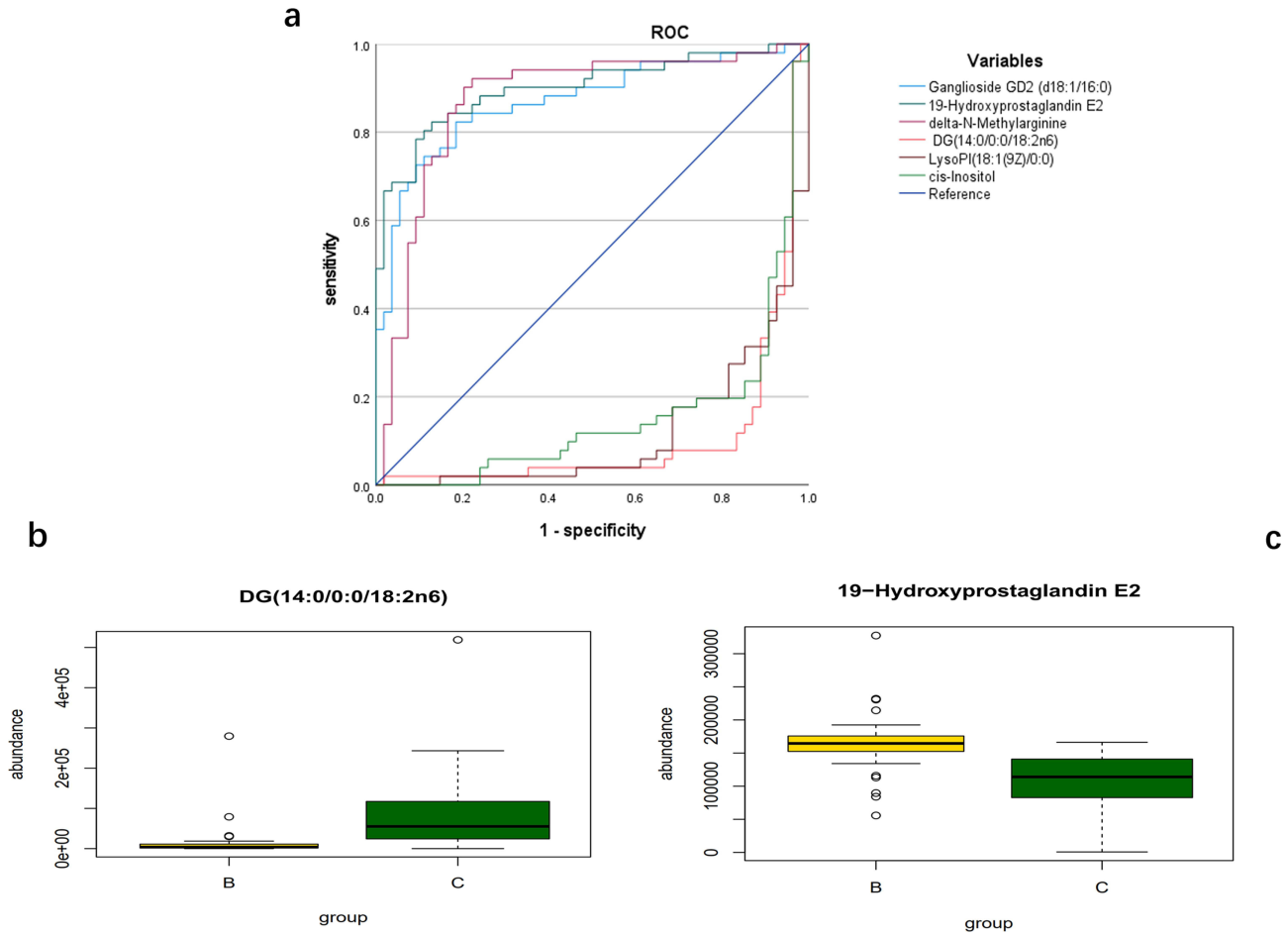

Figure 9 ROC curve and mean plot of metabolites between the GC group and one-week postoperative group. (**a**) ROC curves of the six metabolites; (**b**) mean plots of two differential metabolites.

Abbreviations: ROC, receiver operating characteristics; GC, gastric cancer; B, GC group; C, one-week postoperative group.

the level of phosphatidylethanolamine in GC is higher than in healthy people, but the level of phosphatidylethanolamine decreases after surgery,[21] which is consistent with our result, that the phosphatidylethanolamine level increases in GC. Furthermore, a lipidomics analysis also discovered the difference in phosphatidylethanolamine content between GC tissue and adjacent non-cancerous tissues.[22] Sixth, DG(14:0/0:0/18:2n6) is a diglyceride or a diacylglycerol. A review article discusses the important role of diacylglycerol signaling in the anti-tumor effect. Changes in diacylglycerol activity or abundance

Table 5 AUC of Differential Metabolites Between GC Group and One-Week Postoperative Group

Metabolites	AUC	SE	95% Confidence Intervals	Metabolites
Ganglioside GD2 (d18:1/16:0)	0.871	0.036	0.801	0.941
19-Hydroxyprostaglandin E_2	0.900	0.032	0.838	0.962
Delta-N-Methylarginine	0.870	0.038	0.796	0.945
DG(14:0/0:0/18:2n6)	0.100	0.035	0.038	0.177
LysoPI(18:1(9Z)/0:0)	0.117	0.032	0.054	0.181
cis-Inositol	0.153	0.040	0.075	0.231

Abbreviations: AUC, area under the curve; GC, gastric cancer.

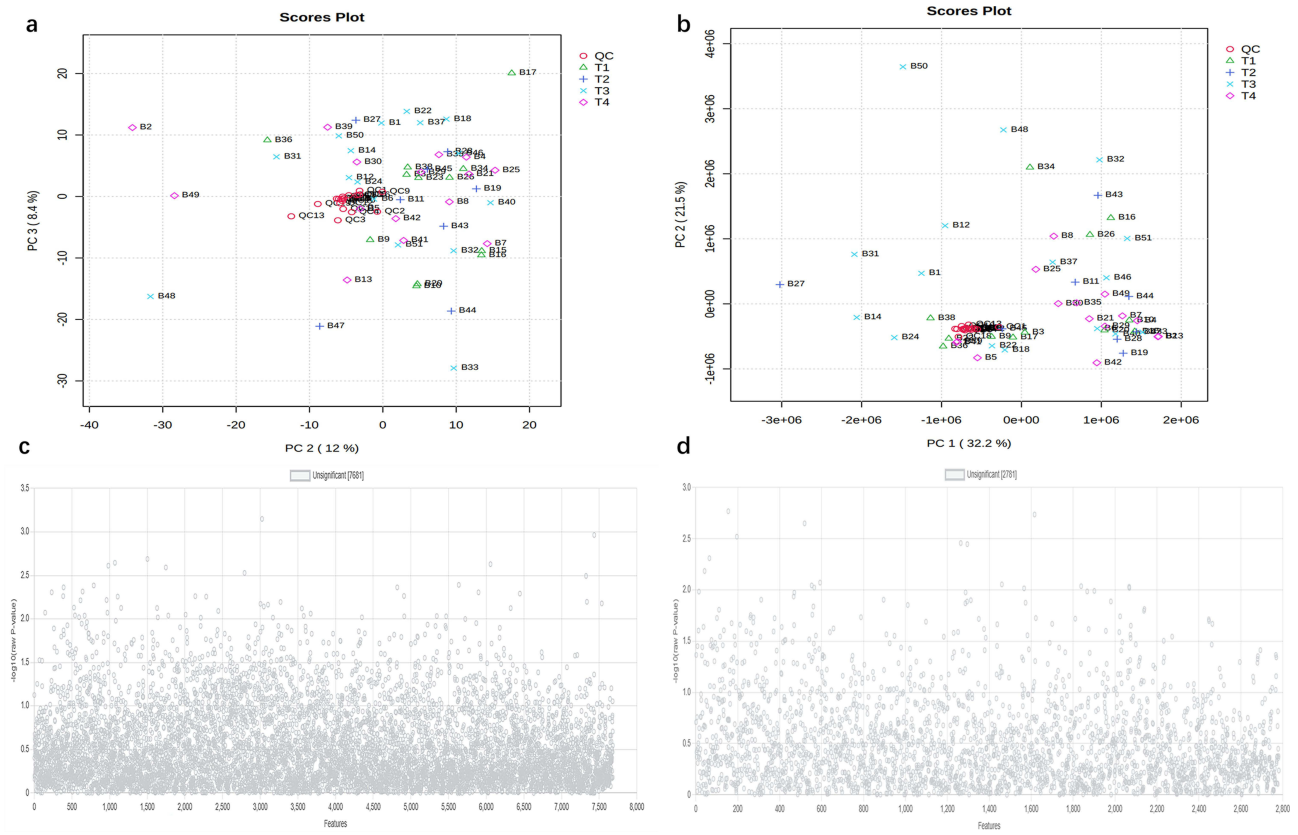

Figure 10 Variance analysis and principal component analysis of samples from T1, T2, T3, and T4. (**a**) Principal component analysis in the positive ion mode; (**b**) principal component analysis in the negative ion mode; each dot represents a single sample; (**c**) variance analysis in the positive ion mode; (**d**) variance analysis in the negative ion mode. The vertical coordinate is the *P* value, the horizontal coordinate is the level of each metabolite, and gray represents the non-significant metabolites with *P*>0.05.
Abbreviation: QC, quality control group.

influence the start, progression, and end of GC, and diacylglycerol could improve T-cell function and enhance tumor immunosurveillance ability.[23] Thus, the diacylglycerol level increases after surgery. Moreover, diacylglycerol loaded in nanomaterials prompts the death of cancer cells via stimulating oxidative stress, which also demonstrates the anti-tumor function of diacylglycerol.[24] Seventh, 19-hydroxyprostaglandin E_2 belongs to the class of organic compounds known as prostaglandins. The tumor microenvironment consists of tumor cells, non-tumor endothelial cells, immune cells, and various signaling molecules, including prostaglandins. The tumor microenvironment is rich in prostaglandins, which could enhance tumor progression via several mechanisms. On the one hand, prostaglandin E_2 could prompt endothelial cell movement, increase the formation of bloods vessel, influence immune cells by upregulating pro-tumor factors and downregulating anti-tumor factors; on the other hand, it could play a synergistic effect with programmed cell death protein-1 to stimulate tumor growth.[25] Prostaglandins are acknowledged mediators between chronic inflammation and gastrointestinal cancer, which hints at the importance of prostaglandins in GC.[26] Therefore, 19-hydroxyprostaglandin E_2 decreases after the tumor has been resected.

There are some strengths to our study. First, the technology of LC-MS possesses high sensitivity and specificity. Second, the use of many statistical methods makes biomarker selection more accurate. Third, the establishment of a prediction mode makes it easier to generalize our results. Fourth, the exploration of differential metabolites between GC and one-week postoperative patients may provide a basis for GC research. However, some limitations must also be mentioned. First, our model lacks external validation because of limited funds. Second, during the selection of subjects for the healthy group in the Medical Examination Center, if we observed that a person's stomach was morphologically normal through endoscopy, we did not further perform endoscopic tissue biopsy, and the person was considered for inclusion in our study. So, the healthy group in this study was not confirmed pathologically as having atrophic gastritis;

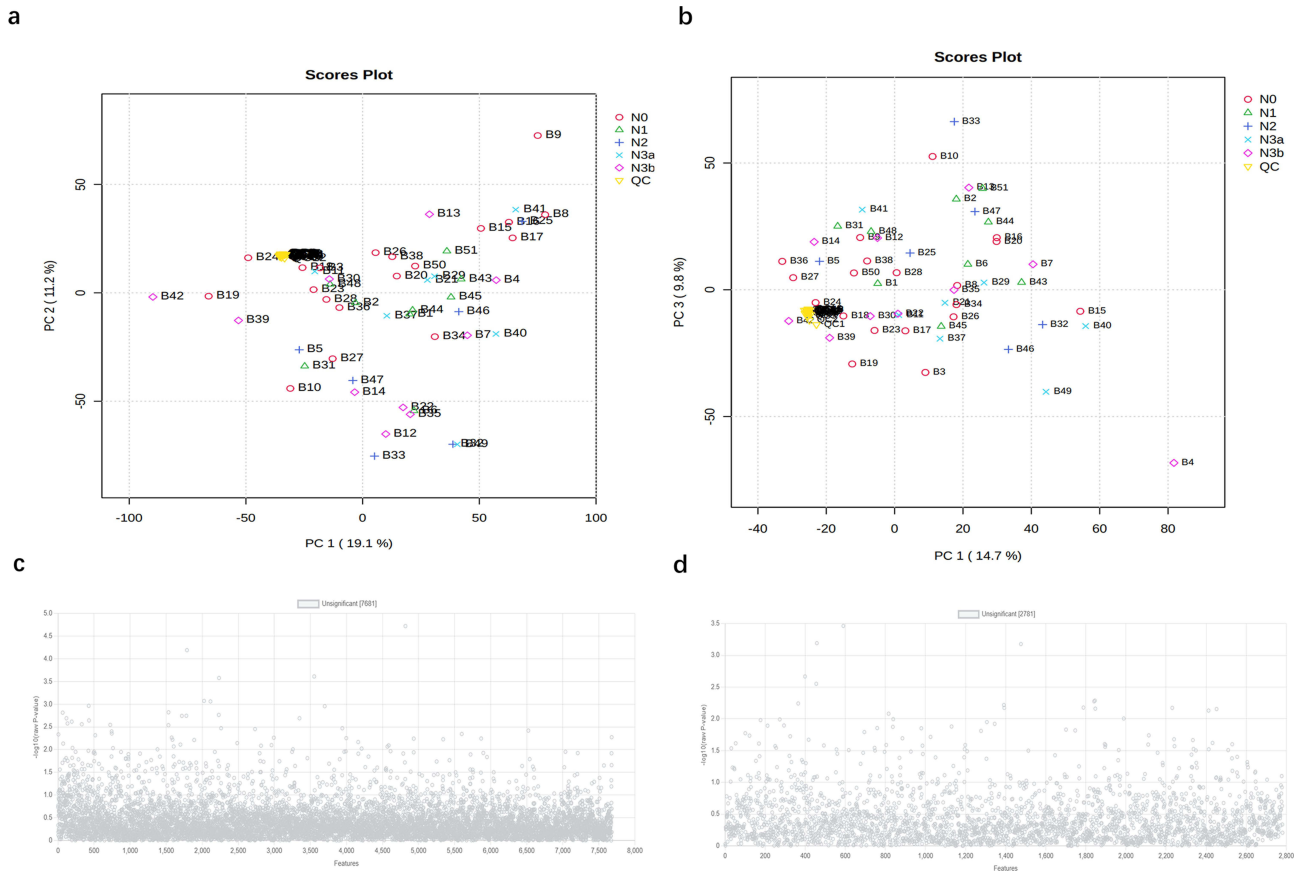

Figure 11 Variance analysis and principal component analysis of samples from N0, N1, N2, N3a, and N3b. (**a**) Principal component analysis in the positive ion mode; (**b**) principal component analysis in the negative ion mode; each dot represents a single sample; (**c**) variance analysis in the positive ion mode; (**d**) variance analysis in the negative ion mode.
Abbreviation: QC, quality control group.

instead, we relied solely on the results of gastric endoscopy to exclude atrophic gastritis. Finally, we analyzed only 152 samples, and more basic studies are needed to verify our conclusions before clinical application.

Conclusion

Differential metabolites were present among three groups. We found four biomarkers in saliva and developed a prediction model for GC, which could be applied as a novel technology to screen for GC, help identify GC as early as possible, and improve patients' prognoses. Furthermore, the changes in two saliva metabolites in postoperative patients could provide important ideas for future studies.

Abbreviations

GC, gastric cancer; CT, computed tomography; LC-MS, liquid chromatography–mass spectrometry; QC, quality control; TIC, total ion chromatography; PLS-DA, partial least squares discriminant analysis; VIP, variable important in projection; SVM, support vector machine; VIF, variance inflation factor; HMDB, Human Metabolome Database; HCA, hierarchical clustering analysis; ROC, receiver operating characteristics; AIC, Akaike information criterion; AUC, area under the curve; GLM, generalized linear model; GOF, goodness of fit; PCA, principal component analysis; MSC, mesenchymal stem cell.

Ethics Statement

The patient sample comes from The First Affiliated Hospital of Jilin University. All patients provided written informed consent, and the study complied with the Declaration of Helsinki.

Acknowledgments

We thank all the patients who took part in this research, all the scholars in this article, and all our teammates for supporting this research. We are also particularly grateful to our colleagues in The First Affiliated Hospital of Jilin University for their contributions.

Author Contributions

All authors made a significant contribution to the work reported, whether that is in the conception, study design, execution, acquisition of data, analysis and interpretation, or in all these areas; took part in drafting, revising or critically reviewing the article; gave final approval of the version to be published; have agreed on the journal to which the article has been submitted; and agree to be accountable for all aspects of the work.

Funding

This work was supported by the National Natural Science Foundation of China (52072142).

Disclosure

The authors declare that the research was conducted in the absence of any commercial or financial relationships that could be construed as a potential conflict of interest.

References

1. Jemal A, Center MM, DeSantis C, Ward EM. Global patterns of cancer incidence and mortality rates and trends. *Cancer Epidemiol Biomarkers Prev*. 2010;19(8):1893–1907. doi:10.1158/1055-9965.Epi-10-0437
2. Tsubono Y, Hisamichi S. Screening for gastric cancer in Japan. *Gastric Cancer*. 2000;3(1):9–18. doi:10.1007/pl00011692
3. Johnston FM, Beckman M. Updates on management of gastric cancer. *Curr Oncol Rep*. 2019;21(8):67. doi:10.1007/s11912-019-0820-4
4. Pedersen AML, Sørensen CE, Proctor GB, Carpenter GH, Ekström J. Salivary secretion in health and disease. *J Oral Rehabil*. 2018;45(9):730–746. doi:10.1111/joor.12664
5. Nonaka T, Wong DTW. Saliva diagnostics: salivaomics, saliva exosomics, and saliva liquid biopsy. *J Am Dent Assoc*. 2023;154(8):696–704. doi:10.1016/j.adaj.2023.05.006
6. Koopaie M, Kolahdooz S, Fatahzadeh M, Aleedawi ZA. Salivary noncoding RNA in the diagnosis of pancreatic cancer: systematic review and meta-analysis. *Eur J Clin Invest*. 2022;52(12):e13848. doi:10.1111/eci.13848
7. Li Q, Ouyang X, Chen J, Zhang P, Feng Y. A review on salivary proteomics for oral cancer screening. *Curr Issues Mol Biol*. 2020;37:47–56. doi:10.21775/cimb.037.047
8. Yan W, Apweiler R, Balgley BM, et al. Systematic comparison of the human saliva and plasma proteomes. *Proteomics Clin Appl*. 2009;3(1):116–134. doi:10.1002/prca.200800140
9. Qiu S, Cai Y, Yao H, et al. Small molecule metabolites: discovery of biomarkers and therapeutic targets. *Signal Transduct Target Ther*. 2023;8(1):132. doi:10.1038/s41392-023-01399-3
10. Liu Y, Zhang Z, Wang J, et al. Metabolic reprogramming results in abnormal glycolysis in gastric cancer: a review. *Onco Targets Ther*. 2019;12:1195–1204. doi:10.2147/ott.S189687
11. Tao Z, Huang C, Wang D, et al. Lactate induced mesenchymal stem cells activation promotes gastric cancer cells migration and proliferation. *Exp Cell Res*. 2023;424(1):113492. doi:10.1016/j.yexcr.2023.113492
12. Ishimoto T, Miyake K, Nandi T, et al. Activation of transforming growth factor beta 1 signaling in gastric cancer-associated fibroblasts increases their motility, via expression of rhomboid 5 homolog 2, and ability to induce invasiveness of gastric cancer cells. *Gastroenterology*. 2017;153(1):191–204.e16. doi:10.1053/j.gastro.2017.03.046
13. Murphy G, Fan JH, Mark SD, et al. Prospective study of serum cysteine levels and oesophageal and gastric cancers in China. *Gut*. 2011;60(5):618–623. doi:10.1136/gut.2010.225854
14. Li J, Tu HJ, Li J, et al. N-acetyl cysteine inhibits human signet ring cell gastric cancer cell line (SJ-89) cell growth by inducing apoptosis and DNA synthesis arrest. *Eur J Gastroenterol Hepatol*. 2007;19(9):769–774. doi:10.1097/MEG.0b013e3282202bda
15. Liu C, Wu Y, Li M, et al. Enantiomer-specific colorimetric tandem assays for salivary d-alanine associated with gastric cancer. *Anal Chem*. 2024;96(5):1906–1912. doi:10.1021/acs.analchem.3c04017
16. Tanner JJ, Fendt SM, Becker DF. The proline cycle as a potential cancer therapy target. *Biochemistry*. 2018;57(25):3433–3444. doi:10.1021/acs.biochem.8b00215
17. Elia I, Broekaert D, Christen S, et al. Proline metabolism supports metastasis formation and could be inhibited to selectively target metastasizing cancer cells. *Nat Commun*. 2017;8:15267. doi:10.1038/ncomms15267
18. Kim HH, Ha SE, Park MY, et al. Identification of kynurenic acid-induced apoptotic biomarkers in gastric cancer-derived AGS cells through next-generation transcriptome sequencing analysis. *Nutrients*. 2022;15(1). doi:10.3390/nu15010193
19. Kim HH, Jeong SH, Ha SE, et al. Cellular regulation of kynurenic acid-induced cell apoptosis pathways in AGS cells. *Int J Mol Sci*. 2022;23(16). doi:10.3390/ijms23168894

20. Choi JM, Park WS, Song KY, Lee HJ, Jung BH. Development of simultaneous analysis of tryptophan metabolites in serum and gastric juice - an investigation towards establishing a biomarker test for gastric cancer diagnosis. *Biomed Chromatogr*. 2016;30(12):1963–1974. doi:10.1002/bmc.3773
21. Zou L, Guo L, Zhu C, Lai Z, Li Z, Yang A. Serum phospholipids are potential biomarkers for the early diagnosis of gastric cancer. *Clin Chim Acta*. 2021;519:276–284. doi:10.1016/j.cca.2021.05.002
22. Hung CY, Yeh TS, Tsai CK, et al. Glycerophospholipids pathways and chromosomal instability in gastric cancer: global lipidomics analysis. *World J Gastrointest Oncol*. 2019;11(3):181–194. doi:10.4251/wjgo.v11.i3.181
23. Cooke M, Kazanietz MG. Overarching roles of diacylglycerol signaling in cancer development and antitumor immunity. *Sci Signal*. 2022;15(729):eabo0264. doi:10.1126/scisignal.abo0264
24. Bae CS, Ahn T. Diacylglycerol in cationic nanoparticles stimulates oxidative stress-mediated death of cancer cells. *Lipids*. 2018;53(11–12):1059–-1067. doi:10.1002/lipd.12124
25. Kobayashi K, Omori K, Murata T. Role of prostaglandins in tumor microenvironment. *Cancer Metastasis Rev*. 2018;37(2–3):347–354. doi:10.1007/s10555-018-9740-2
26. Wilson DJ, DuBois RN. Role of prostaglandin E2 in the progression of gastrointestinal cancer. *Cancer Prev Res*. 2022;15(6):355–363. doi:10.1158/1940-6207.Capr-22-0038